Spatio-temporal wildfire risk assessment, power grid resilience, proactive de-energization, stochastic wildfire ignition maps, power system wildfire metrics.

Accepted for publication in IET Generation, Transmission & Distribution, January 2022

IET Generation, Transmission & Distribution,

Research Article

IET Journals
The Institution of Engineering and Technology

Data-Driven Spatio-Temporal Analysis of Wildfire Risk to Power Systems Operation

ISSN 1751-8644
doi: 0000000000
www.ietdl.org

Amarachi Umunnakwe[1], *Masood Parvania*[2], *Hieu Nguyen*[3], *John D. Horel*[2], *Katherine R. Davis*[1]

[1] *Electrical and Computer Engineering, Texas A&M University, College Station, TX, USA*
[2] *University of Utah, Salt Lake City, UT, USA*
[3] *North Carolina Agricultural and Technical State University, Greensboro, NC, USA*
** E-mail: amarachi@tamu.edu, masood.parvania@utah.edu, htnguyen1@ncat.edu, john.horel@utah.edu, katedavis@tamu.edu*

Abstract: Wildfires are natural or man-made disasters that continuously threaten portions of the transmission and distribution grid, and thus the stability of the electric grid. This paper presents a two-stage framework for assessing power system-wildfire risk using a data-driven wildfire prediction model. The first stage of the framework estimates the spatio-temporal probability of potential wildfire ignition and propagation using a deep neural network in combination with the wildfire physical spread model. Analysis reveals similar spatial and temporal patterns between the model-predicted wildfire ignition potential and actual wildfire ignition. Motivated by these observations, the second stage assesses the wildfire risk in the power grid operation in terms of potential loss of load by de-energization, through combining geospatial information system (GIS) data of the power grid topology and the stochastic spatio-temporal wildfire model developed in the first stage. The electric power utility applications introduced by the proposed framework are twofold: 1) a spatio-temporal risk model for proactive de-energization against potential power system failure-induced wildfire, and 2) a spatio-temporal spreading model for optimal grid operations against exogenous wildfire. The proposed model, based on real-world dataset, is demonstrated on the IEEE 24-bus test system mapped to a study area in northern California, while the results illustrate the proposed model can achieve the best performance in potential wildfire ignition detection (AUC of 0.995) compared to other baselines, as well as demonstrates the risk-aware operation of the power system enabled by the proposed framework.

1 Introduction

THE increasing magnitude and frequency of power outages induced or motivated by wildfires affects the operation of critical services and leads to lost opportunity costs [1]. The California Department of Forestry and Fire Protection estimates damages from the 2018 Woolsey and Camp fires to be about $4 and $11 billion respectively [2], with Campfire responsible for about 84 deaths [3]. Additionally, wildfire threats in October 2018 and 2019 led Pacific Gas and Electric (PG&E) to shut off power to a sizeable number of customers in extreme risk areas of northern California leading to lost opportunity costs when no wildfires occurred [4]. Subsequently, the 2020 Zogg fire saw PG&E facing 31 criminal charges, including manslaughter, for the utility's role in the fire that claimed 4 lives and destroyed more than 200 building properties [5]. More recently, the 2021 Dixie fire was caused by the blowing of two fuses when a Douglas fir fell on a PG&E line [6]. The fire gulped more than $630 million in suppression efforts and led to tangible losses including damages to approximately 1500 residential and commercial property, injuries and fatalities [7].

1.1 Background and Motivation

In response to wildfire threats, utilities have significantly invested on wildfire monitoring systems and analytical tools, which generally rely on observations from remote automated weather stations to evaluate current weather conditions [8] that are disseminated and retrieved [9] from many sources such as Synoptic's Mesonet API. These data are then used to estimate and strategize for optimal operation in the face of wildfire threats, but with room for improvements. In fact, the decisions of a utility to shut off power to more than sixty thousand northern California customers in 2018 and nearly a million in 2019, was controversial [10]. It may be, however, impossible to assess if this was an overestimation of impact and utility resources ("conservative"), but the passing of the California Senate Bill 901 required states investor-owned utilities with the California Public Utilities Commission to file wildfire mitigation plans, increasing research on the topic [11].

Conventionally, electric power utilities have often performed fundamental analysis to indicate wildfire threat alert on coarse resolutions of spatial areas while not utilizing the richness of historical data, evident in indices such as the Fire Potential Index [12]. This index, for instance, utilizes a linear summation of present weather variables and fuels to provide threat levels (extreme, elevated, normal) for predefined regional-scale threat areas. This may arguably lead to over-estimation of risk, over-allocation of operational resources, and consequently "conservative" risk analysis for utilities.

1.2 Literature Review

Studies on wildfire prediction and estimation [13–15] have mainly focused on numerical quantification [16] and fire scale [17], often using techniques such as regression [18], in an effort to aid mitigation. In [19], wildfire variables are studied to predict spatial patterns of ignition producing national-level ignition risk maps. To aid pre-wildfire planning, [20] implements fire danger mapping system based on numerical weather prediction and derived moisture content of live fuels. Historical data for vegetation, climate and locational features have been utilized in [21] to predict the risk of wildfire ignition. However, these region-specific wildfire models are simply aggregated over space or time with approximated/linear and spatially constant effects [22]. Hence, their accuracy can be affected by the limited integration of the non-linear influence of variables, and similarly, do not fully utilize recent wildfire monitoring investments of grid utilities. Wildfire risk prediction has also been done where model performance using machine learning approaches have been evaluated [23]. Artificial intelligence techniques have also been effective for wildfire analysis and outperform conventional statistical methods [24–26]. Additionally, interactive maps have been garnering literary and industry application to supply information on wildfires in real-time. For instance, in [27], a real-time fire prediction

Accepted for publication in IET Generation, Transmission & Distribution, January 2022

system is developed for visualizing wildfire risk at specific locations based on a machine learning model. Although these methods prove effective, they generally have not been designed to integrate with the power grid operations.

The effect of this on the power system side is the assumption of already progressing wildfires, while geographical uncertainties of spatio-temporal variables are often assumed [28] and not investigated. For instance in [29], energy dispatch is optimized assuming an already progressing wildfire. The same progressing wildfire assumption is applied in[30] to dynamically change thermal ratings of power lines and in [15] to optimize resource preparation.

1.3 Approaches, Contributions, and Paper Structure

This paper develops a deep learning based framework for analyzing the expected spatio-temporal impacts of stochastic wildfire threat on the power grid. The proposed framework, as shown in Fig. 1, integrates a detailed spatio-temporal wildfire analysis model to evaluate system risk. The model incorporates information from real databases towards potential wildfire ignition maps, as the spatio-temporal wildfire "readiness" of a location does not necessarily imply an ignition until a fire source is applied. Therefore, a model is proposed to estimate the spatio-temporal probability of a potential wildfire ignition which can be applied to power transmission and distribution systems. The advantage in modeling potential ignitions pre-wildfire is to prepare for critical scenarios and proceed with optimal strategies to better mitigate risks arising from extreme wildfire events, thereby reducing the propensity of outages and power shutoff to customers. As wildfires can be caused by power system failure or by exogenous causes (human, natural events), the applications of the estimation result are twofold. First, it provides spatio-temporal risk for proactive de-energization against potential power system failure-induced wildfire [28]. Second, it generates a spatio-temporal spreading model for optimal grid operations against potential exogenous wildfires [15]. Depending on the application, risk metrics quantifying potential wildfire operational impact, power utility response time for mitigation, and strategy-enabling metrics for mitigation vs. restoration, are developed in the second-stage. In summary, the main paper contributions are as follows:

- We develop a comprehensive spatio-temporal wildfire risk analysis framework using a data-driven deep learning approach that efficiently incorporates publicly-available historical wildfire and GIS data for estimating wildfire ignition risk and its impact on power grid.
- Novel quantitative risk metrics that capture potential effects of fuel, vegetation, and wind speed, on wildfire propagation are proposed, while the weighted impacts of wildfire predictive variables are furnished to serve utility operations and stakeholder strategies.
- The framework can provide information to power utilities towards optimizing the grid operation, i.e., the proactive de-energization to prevent endogenous power system failure induced wildfire and the response strategy e.g., "let-burn", against exogenous wildfire threats.

The rest of the paper is organized as follows: overview of the proposed spatio-temporal framework is outlined in Section 2 where the geographical formulation and data requirements are also discussed. In Section 3, the wildfire estimation model is discussed and the result utilized in the power grid risk assessment model as presented in Section 4, which also develops the quantitative power system risk metrics. Simulations are conducted and numerical results are illustrated on the IEEE 24-bus test system as presented in Section 5, while the conclusions are drawn in Section 6.

2 Overview of the Proposed Model

Wildfires are influenced by a number spatial and temporal factors that can be unique in different geographical locations which can lead to inaccuracies in specified mathematical models. Hence, the objective of the proposed framework is to drive operational strategy with data-driven situational awareness to wildfire. As in Fig. 1, the framework consists of two sequential stages. First, the *spatio-temporal wildfire estimation model* predicts the probability of potential wildfire ignition, utilizing the spatio-temporal wildfire ignition probability predictor model (STWIP), and estimates potential wildfire spread, producing important parameters such as ignition probability maps and the rate of spread of potential ignitions to critical power components. These parameters are then passed to the proposed *power grid wildfire risk assessment model*, which aims to optimize power system operations and risk assessment such that outage cost is minimized. The risk assessment model optimizes power system operations by GIS-enabled mapping of these parameters to the power network and generating wildfire threat scenarios. Part of the risk assessment model also includes proposed power system-wildfire metrics that enable optimal operational strategies such as choosing mitigation vs. restoration ("let-burn"). Both stage 1 and stage 2 models incorporate effective wildfire analysis, enhancing power system resilience, reduction in customer outages and hence, operational cost during wildfire threats. The rest of this section discusses the structure of the proposed model and data requirements, while the spatio-temporal wildfire estimation and power grid wildfire risk assessment models are discussed in detail in the next two sections.

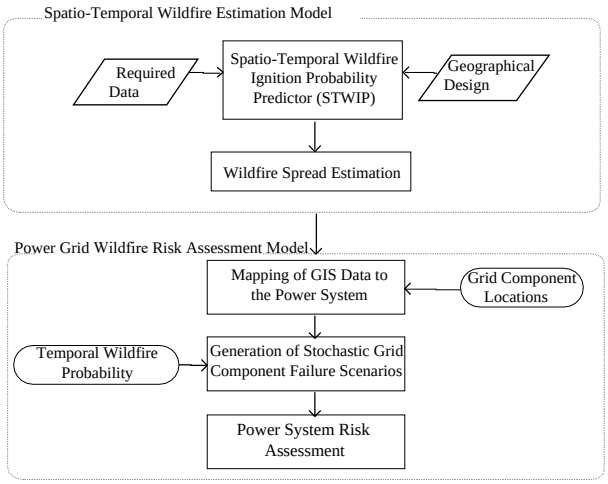

Fig. 1: Structure of spatio-temporal wildfire risk assessment model

2.1 Geographical Structure of the Model

A spatial location is a point i with geospatial coordinate $i.loc$ defined by a latitude and longitude *(lat,lon)* at any location in a grid cell. The grid cells here are 3km $\times$ 3km polygons which have uniform past spatio-temporal wildfire characteristics and a centroid. Each grid centroid also has geospatial coordinates $g_c.loc$. For instance, the past spatio-temporal characteristics of a historical sample ignition occurred in i is obtained by its association with $g_c.loc$ of the grid cell $g \in G$ in which it is situated, since the centroid is processed to bear the characteristics of g. Each grid has a set of historical wildfire ignition events with geospatial coordinates $i.loc$. These historical events, which form sample points in the training data, have a set of variables, $\mathbf{x} = [x_1, x_2, ..., x_D]$, obtained for their unique $i.loc$ and dates of ignition. Here, D denotes the dimensionality. These wildfire-informative variables are referred to as Wildfire Predictor Variables (WPVs) and are usually sourced from weather stations geographically situated at locations of interest. Their interactions and correlation can be modeled towards wildfire prediction. They can vary spatially and/or temporally, are indicative of wildfire occurrence, and are often called explanatory variables [31].

Accepted for publication in IET Generation, Transmission & Distribution, January 2022

2.2 Data Requirements

The proposed framework proceeds with data pre-processing and integration (solid green arrows), feature extraction and training the predictor (solid black arrows), these precursors are as illustrated in Fig. 2 and discussed as follows.

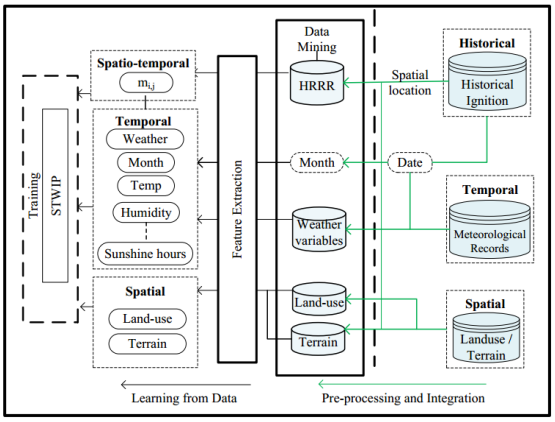

Fig. 2: Spatio-temporal wildfire prediction model

2.2.1 Data Pre-processing: This stage proceeds with obtaining the grid centroids together with spatial data e.g., land-use and terrain data, from databases such as the National Oceanic and Atmospheric Administration's High Resolution Rapid Refresh (HRRR) model [32]. The temporal probabilities, π_j of wildfire ignition, as shown in Appendix 8.4, are also calculated in this stage from the US Geological Survey historical ignition data and can be used as a feature to improve estimation. This assumption of a same climate period is enabled by the similarity in the data distribution over the historical period of analysis as illustrated in Appendix 8.2, Fig. 14. Also in this phase, the python scrapper is coded to request and clean meteorological data for unique spatial locations on days of interest. These days of interest depend on user applications but for this work, meteorological variables on historical ignition and non-ignition days are duely processed for training/validation of the predictor while forecasted meteorological variables are requested for days that wildfire potential is to be predicted.

2.2.2 Data Integration: The next phase is data integration which proceeds in two levels. The first is the spatial integration, where $i.loc$ of historical ignitions are associated to $g_c.loc$ to obtain the past ignition characteristics of g. The goal here is to enable spatial locations in the training data inherit wildfire attributes of the grid cell in which they are located. The second occurs after feature extraction during integration into python's pandas dataframes in preparation for training. This dataframe is a two dimensional data structure with columns of multivariate data. The month in which the training ignition sample occurred is incorporated as a feature to account for temporal relation of features, and is also critical to the utilization of only one fundamental deep network.

2.2.3 Feature Extraction:

Past Spatio-Temporal Ignition: This feature captures sequential changes in characteristics of spatial wildfire ignition over time and is crucial in the capability of the predictor to use one fundamental deep network. It is calculated from the historical wildfire database and is the initial (historical) ignition probability of a spatial location in the same climate period. To this end, we compute the past wildfire ignition probability $m_{g,j}$ of a grid cell g in period j of our comprehensive year. Since this attribute is inherited by all i in grid cell g, we refer to this attribute as $m_{i,j}$. Specifically, because the climate pattern of the multiple-year-dataset is assumed constant, the conditional probability of an ignition occurring in grid cell i given the study area, is used to calculate $m_{i,j}$ given that grid cells are a subset of the studied geographical area as in (1).

$$m_{i,j} \approx \frac{n_{g,j}}{N}, \tag{1}$$

where $n_{g,j}$ is the total number of wildfires occurred in cell g in period j, and N is the total number of wildfires that occurred in the multiple year period. Assuming constant climate, the multi-year period (e.g., 1996-2016) can be modeled as a comprehensive year. As mentioned earlier, in order to enhance the computation of $m_{i,j}$ considering the scarcity of historical ignitions in some grid cells, the Monte Carlo population technique is employed in pre-processing the original dataset to further populate grid cells.

Temporal (Meteorological) Features: Wildfire occurrence is influenced by non-linear and complex meteorological features which are temporally related. Temporal meteorological input includes temperature, rain, humidity, sunshine hours. The choice of these features are informed by indices such as the Angstrom, Nesterov, and Canadian Forest Fire Weather Index as well as the US Fire Danger Rating System [33].

Spatial (Static) Features: These features characterize spatial locations for same climate periods and are influential to wildfire occurrence [34]. Spatial data of land-use and terrain can be obtained from sources such as the HRRR model which have standard grid points that can serve as grid centroids and enable division of the studied geographical area into grid cells with the same spatial and spatio-temporal features. Historical ignition events that fall within a grid cell are used to obtain $m_{i,j}$ of the respective cells which are in turn inherited by the sample points i within g, during training.

In addition, the past ignition probability and ignition month are also included as spatio-temporal and temporal features respectively. Additional details can be found in Appendix 8.1 and 8.3.

2.2.4 Data construction: Here, we discuss the logic behind constructing the training data as there is little to none pre-existing for wildfire analysis. Since training samples are based on historical ignition/non-ignition days, the dates (dd/mm/yy) and corresponding $i.loc$ are extracted from the historical ignition database and are utilized to automatically request training sample variables. Once the features are extracted from obtained variables, this training sample point is assigned with a classification label 1, meaning the historical status of ignition was active for the sample. Next, the feature data are requested for the same $i.loc$ and another (dd/mm/yy) prior to the active ignition date, when no wildfire ignitions were reported to have occurred and this is labelled a 0, meaning that the historical status of ignition was inactive for the sample. In particular, the ignition label for a training sample is defined as:

$$Ign = \begin{cases} 1, & \text{if} \quad ign_{(j)}\ recorded \\ 0, & \text{if} \quad ign_{(j-n)}\ \neg recorded \end{cases} \tag{2}$$

where Ign is the historical wildfire ignition status in day j, and $n = \{1, 2, ..., 30\}$ depending on any day in the given month and year where an ignition was not recorded. This process constitutes the dataframe for training the STWIP. For the 0-labelled samples, dates prior to ignition (1-labelled sample) of an $i.loc$, are chosen since historical ignition could have significantly tampered with temperature, fuel and vegetation, rendering later dates deceptive for use as 0-labelled training samples. It is worth noting that although we assume true absence points, these 0-labelled samples are pseudo-absence points since it is unknown if ignition could not occur (there was no potential for ignition) or simply did not occur (there was no source of ignition) in that historical date and $i.loc$.

3 Spatio-Temporal Wildfire Estimation Model

After data construction, the dataframe is fed into STWIP as input data following some transformations discussed herein. The input

IET Generation, Transmission & Distribution, pp. 1–13

Accepted for publication in IET Generation, Transmission & Distribution, January 2022

data is cleaned, missing values are filled with an average of their nearest neighbors. A major part of training data processing includes rescaling the features to have the properties of a standard normal distribution ($\mu = 0, \sigma = 1$). The need for rescaling arises as features are multivariate with different units. Also, since feature magnitudes in instance $\mathbf{x}_i$ play a role in the updates applied to the weights during gradient descent, rescaling becomes important. This standardization is implemented using the Z-score as follows:

$$z = \frac{x - \mu}{\sigma}. \tag{3}$$

Then STWIP predicts the expected ignition potential of a spatial location in period j as discussed further.

3.1 Spatio-Temporal Wildfire Ignition Probability Predictor

The aim is to train a neural network with the problem objective formulated as follows. Given a collection of sample points i with geospatial coordinates $i.loc$ of *(lat,lon)* $\in$ historical ignition data, where features of the sample point i are known, we aim to predict the potential of a wildfire ignition at periodic intervals. We propose a model based on supervised learning of spatial, spatio-temporal and temporal features to capture complex and non-linear interactions between WPVs using a deep neural network (DNN). The DNN is the prediction algorithm of the STWIP and unlike traditional methods of wildfire estimation with simple logistic regression [18, 35], the DNN is capable of modeling non-linear correlations between the WPVs as illustrated in (4), and can update the network's basis functions in specific input space directions.

$$\widehat{y} = \sigma\left(\sum_{h=1}^{H} w_{oh}^{T} h\left(\sum_{i=1}^{D} w_{hi}^{T} * x_i + w_{h0}\right) + w_{o0}\right), \tag{4}$$

where $\mathbf{w}$ is the vector of adjustable weight parameters, with input variables x_i, σ is a threshold function, and $\{i, h, o\}$ represent the input, hidden, and output layers. By adjusting the weight vector through different training epochs the predicted labels are mapped closer to the target labels, estimating the probability of potential wildfire ignition, $\pi_{i,j}$, as follows:

$$\pi_{i,j} = f(\mathbf{x}). \tag{5}$$

The STWIP architecture is a three layer fully connected network as shown in Fig. 3, utilizing the Adam optimizer, ReLU activation, and softmax activation at the output layer. The hidden layers' (12,3)

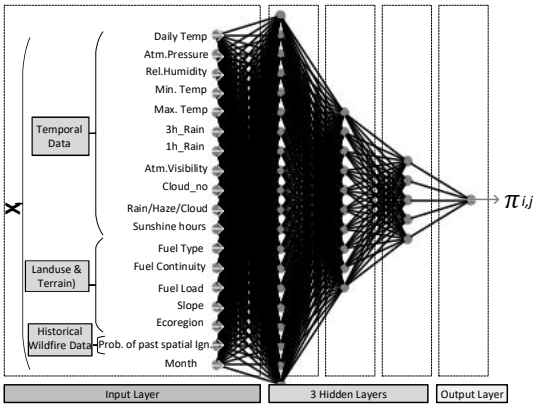

Fig. 3: Inputs and predicted output

neurons, respectively, are chosen to avoid over-fitting and enhance prediction accuracy.The data input, $\mathbf{x}$, is fed into the input layer. The output layer consists of two neurons that output probabilities of potential ignition/non-ignition in one hot encoded format. The network is trained and minimized over the cross-entropy loss. The trained STWIP is illustrated in Algorithm 1 in Appendix 8.5.

3.2 Wildfire Spread Estimation

In modeling wildfire behaviors including spread, software such as Prometheus and Burn-P3 have been developed, but however, may require predefined inputs such as initial ignition grids from all historical fires, the different ecoregions, percentage of escaped fires and more, which may not be readily available to the user. In literature, models such as the FLAME [36] have been developed to rely on observable field assessments to consider areas of high fire spread rates. In [37, 38], the developed model seeks to attain the fire front using a variation of the Thomas Equations shown in (6) and (7).

$$V^f = \frac{k(1 + V_w)}{\rho_b} \tag{6}$$

$$r^f_{i,j,\omega,t} = r^f_{i,j,\omega,t-1} + V^f_{\omega,t}\, \Delta t\, cos(\phi^{\omega}_{i,j,\omega,t}) \tag{7}$$

where V_w is wind speed, k is fire-type parameter, ρ_b is the bulk density, r^f is the radius from the initial ignition point to the fire boundary, and ϕ^w is wind direction.

However, if a wildfire ignites in a cell i in period j, its spread rate depends on surrounding fuel types and wind speed, which can be captured by the wildfire-fuel spread characteristics. Hence, we adapt an approximate radial spread rate using the FireLine Assessment MEthod [36], that can be determined by assessing the fuel type and wind speed at each HRRR grid point nearest to the potential wildfire ignition location. In this paper, instead of arbitrary values of spread rates, practical datasets that adapt the considered geographical area to different fuel types is utilized. The study area is

Table 1 Relating the land-use features to fuel type

Value	Label	Fuel	Study Area Coverage
1	Evergreen Needleleaf forest	Litter/Crown	46.139%
2	Evergreen Broadleaf forest	Litter/Crown	0.000%
3	Deciduous Needleleaf forest	Litter	0.000%
4	Deciduous Broadleaf forest	Litter	0.000%
5	Mixed forest	Litter/Crown	0.000%
6	Closed shrublands	Litter/Crown	0.000%
7	Open shrublands	Litter/Crown	0.000%
8	Woody savannas	Grass	11.611%
9	Savannas	Grass	14.306%
10	Grasslands	Grass	9.583%
11	Permanent wetlands	Barrier	0.000%
12	Croplands	Barrier/Grass	17.028%
13	Urban and built-up	Barrier	0.722%
14	Cropland/Natural vegetation mosaic	Barrier/Grass	0.000%
15	Snow and ice	Barrier	0.000%
16	Barren or sparsely vegetated	Barrier	0.028%
17	Water	Barrier	0.583%
18	Wooded Tundra	Litter/Crown	0.000%
19	Mixed Tundra	Grass	0.000%
20	Barren Tundra	Barrier	0.000%

mapped, by a consulted fire expert, Robert Ziel, to three common fuel types namely crown, litter, and grass as illustrated in Table 1 which also shows the coverage of each fuel type in our study area in northern California. Hence, this paper considers three common vegetation/fuel types (crown, litter, and grass) with spread rates modeled as a function of wind speed, W, as in (8) and as shown in Fig.4. Note that in the case of multi-fuel types such as litter and crown, the fuel type with higher spread rate was chosen. Constant but atypical wind speed directed towards the power system components is assumed, in order to account for the worst case scenarios of wildfire spread in the spatio-temporal assessment.

$$\begin{aligned} \omega_{\mathsf{grass}} &= 14.4(W)^{1.232}, \\ \omega_{\mathsf{crown}} &= 4.87(W)^{1.146}, \\ \omega_{\mathsf{litter}} &= 1.03(W)^{1.213}. \end{aligned} \tag{8}$$

Accepted for publication in IET Generation, Transmission & Distribution, January 2022

Armed with the potential rate of spread of the wildfire, utilities are able to optimize operations based on parameters such as expected distance and the time it takes a potential ignition to reach critical grid components.

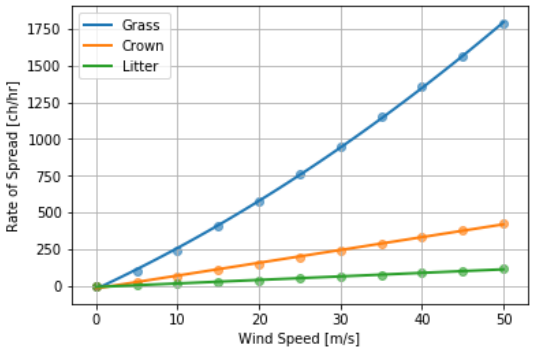

Fig. 4: Rate of Spread as a Function of Wind Speed (1 ch/hr = 0.005588 m/s)

4 Power Grid Wildfire Risk Assessment Model

This section presents the proposed model for the power grid risk assessment, utilizing the outputs of wildfire estimation model presented in Section 3. The wildfire potential ignition map (ignition probability map), produced by the STWIP, aids in proactive de-energization to prevent endogenous fires caused by power system failure [28] while the spread estimation aids improvement in adaptive operation of power grid against exogenous wildfires [15]. Specifically, a set of grid component outage scenarios are first generated by incorporating the output parameters of the first stage estimation model with GIS information of the power grid. In particular, given $\pi_{i,j}$, scenarios are sampled given the distribution of the wildfire potential ignition map and potential ignition locations, generating expected scenarios for the power system risk assessment model. Note that the granularity of $\pi_{i,j}$ can be improved to hourly depending on user application. In this paper, we estimate the hourly probabilities from $\pi_{i,j}$ as follows:

$$(1 - p_{i,h})^H = (1 - \pi_{i,j}) \tag{9}$$

where $p_{i,h}$ is the hourly probability of potential wildfire ignition in i, and H is the cardinality of hours in day j. Based on these scenarios, three risk metrics, namely, critical response time, scenario based damage cost, and the expected damage cost are calculated to assess risk.

4.1 Power Grid Outage Scenario Generation

We aim to generate the outage scenario of grid component c at time t of operational day j of the year. Assume that the wildfire ignition happens at time $t^* = 0$, and we aim to assess the operation of power grid for the subsequent 24 hours after the potential incident. In other words, the utility operator's thought process is: "if the potential wildfire occurs given scenario, s, and I have knowledge of the spread rates given s, I should estimate what component outages can be induced or motivated by this fire so I can be better prepared for such scenarios". Let π_s denote the probability of occurrence of scenario s corresponding to a set $\mathcal{I}_j^s$ of potential ignition locations of day j. The spreading rate ω_i^s of the ignition in location i in scenario s is obtained by using the spread model presented in Section 3.B with the corresponding values of forecast wind speed and fuel types around i. The GIS data of the power grid is mapped into the considered area. The characterization of a wildfire induced (exogenous) grid outage scenario is illustrated in Fig. 5. In particular, the component (e.g., transmission line) is assumed to be damaged if the potential fire crosses its safety zone defined by Δ_c and the status of power grid component c is characterized by a scenario dependent parameter $\delta_{c,t}^s$ as:

$$\delta_{c,t}^s = \begin{cases} 0, & \text{if } \min\limits_{i \in I_j^s} D_c^i - \omega_i^s \Delta t > \Delta c \\ 1, & \text{if } \min\limits_{i \in I_j^s} D_c^i - \omega_i^s \Delta t < \Delta c \end{cases} \tag{10}$$

where $\Delta t = t - t^* = t$ ($t^* = 0$) is the potential duration of the wildfire spread, D_c^i is the Euclidean distance from the potential ignition point i to the grid component c, and $\omega_i^s \Delta t$ is the spreading radius of the wildfire from its ignition point. Note that (10) considers potential wildfire ignition with spread closest to component c, since multiple ignition points can possibly occur in a scenario s, which was reportedly the case in the infamous Campfire. Also, when a component is on outage ($\delta_t^s = 1$), we assume it continues to be out until the end of the considered operation horizon. The value of Δ_c can be adapted from numerical determination of the Acceptable Safety Distance [39], which furnishes a detailed thermodynamics of wildfire effect on system components, informed by flame characteristics and a vulnerability threshold. The safety distance is informed by flame characteristics and a vulnerability threshold, and is the distance between the transmission line and the fire at which the thermal radiative flux is less than a given threshold, Φ_{thresh}. The threshold value is set to the vulnerability of transmission lines. The safety adapted distance is determined by the following correlation:

$$D_x(opt) = D^{\text{I}} \left(1 - exp\left(-p_{thresh} \tfrac{2L}{l_f}\right)\right), \tag{11}$$

where p_{thresh} is a pre-determined empirical parameter for each Φ_{thresh}, l_f is the flame length, $2L$ is the width of fire, and

$$D^{\text{I}} = \frac{l_f cos\gamma \sqrt{-4\Phi_{thresh}^2 + (BT_f^4 \varepsilon\tau)^2}}{2\Phi_{thresh}} + I_f sin\gamma, \tag{12}$$

where τ is the atmospheric transmissivity, ε represents flame emissivity, B is the Boltzmann constant, and T_f is the average temperature of the flame.

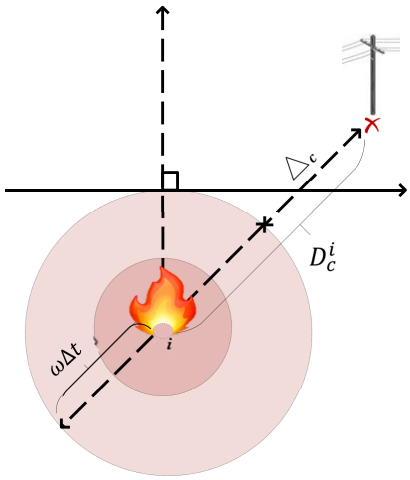

Fig. 5: Wildfire-induced outage scenario generation

4.2 Metrics for Power Grid Wildfire Risk Assessment

The following metrics are developed to aid utility decision making process and operational strategies in the wake of a wildfire threat. Note, since the metrics are used for a particular operation day j of the grid, we omit the notation j from hereon for simplifying the notation.

IET Generation, Transmission & Distribution, pp. 1–13

Accepted for publication in IET Generation, Transmission & Distribution, January 2022

4.2.1 The Critical Response Time ($\overline{\Delta t}$): This metric furnishes the time period within which utility operators can make operational changes to minimize economic damages before power shutoff is absolutely necessary. It is a function of the distance from the potential wildfire ignition point i to power system component c (see Fig. 5), and the wildfire rate of spread ω_i^s as follows:

$$\overline{\Delta t} = \min_{\forall i \in I^s, s \in \mathcal{S}} \frac{D_c^i - \Delta_c}{\omega_i^s}. \tag{13}$$

Note the importance of this metric since aspects of vegetation, fuel, and velocity of wildfire spread, based on the spreading model in (8), is incorporated into a time measure for optimizing utility actions pre-wildfire. The metric inadvertently provides a time estimate before the potential ignition will pose a risk, and serves in two ways depending on application. First, if $\overline{\Delta t}$ is $<<$ threshold (utility defined, associated with Δ_c), then ignitable location is close to the power system component, ignition is possible within Δ_c and components should be de-energized to avoid being sources of ignition for endogenous wildfires. Secondly, if $\overline{\Delta t}$ is $>>$ threshold i.e., distance of potential ignition is far enough from component, the utility can afford to wait pre-wildfire and not cut off power to customers, say H hours before actual ignition, which is mainly where revenue is lost during wildfire threats [10]. Also for the latter depending on the critical time, utilities can operate and strategize before any potential exogenous wildfire fronts induce component outages.

4.2.2 The Scenario based Damage Cost: The operational damage cost of a particular scenario s is the result of the optimal response of the power grid against the realized outage scenario. The operational damage cost includes losses in revenue accruing to the power utility due to lost opportunity costs arising from load curtailment, including power shutoff to customers and intended unavailability of power components, e.g., power lines, from wildfire threats. In the case of the power transmission grid, such scenario based damage cost can be defined as the optimal value of the following security constrained optimal power flow as below:

$$\text{cost}_s = \min \sum_{t \in T} \sum_{b \in \mathcal{B}} \text{VOLL}_{b,t} \text{LC}_{b,t}^s. \tag{14}$$

$$\text{s.t.} \quad P_{l,t}^s = \frac{\left[\theta_{b,t}^s - \theta_{b',t}^s\right]}{x_l}(1 - \delta_{l,t}^s), \ \forall l = bb' \in \mathcal{L} \tag{15}$$

$$P_{g,b,t}^s - P_{d,b,t} + \text{LC}_{b,t}^s = \sum_{bb' \in \mathcal{L}} P_{bb',t}^s, \tag{16}$$

$$0 \le \text{LC}_{b,t}^s \le P_{d,b,t}, \ \forall b \in \mathcal{B}, \forall t \in \mathcal{T} \tag{17}$$

$$(1 - \delta_{g,b,t}^s)\underline{P}_{g,b} \le P_{g,b,t}^s \le (1 - \delta_{g,b,t}^s)\overline{P}_{g,b}, \quad \forall g \in \mathcal{G}, \forall b \in \mathcal{B}, \forall t \in \mathcal{T} \tag{18}$$

$$-(1 - \delta_{l,t}^s)\overline{P}_l \le P_{l,t}^s \le (1 - \delta_{l,t}^s)\overline{P}_l, \quad \forall l \in \mathcal{L}, \forall t \in \mathcal{T} \tag{19}$$

$$\underline{\theta}_b \le \theta_{b,t}^s \le \overline{\theta}_b \quad \forall b \in \mathcal{B}, \forall t \in \mathcal{T}, \tag{20}$$

$$P_{g,b,t}^s - P_{g,b,t-1}^s \le RU_{g,b}, \ \forall g \in \mathcal{G}, \forall b \in \mathcal{B}, \forall t \in \mathcal{T}, \tag{21}$$

$$P_{g,b,t-1}^s - P_{g,b,t}^s \le RD_{g,b}, \ \forall g \in \mathcal{G}, \forall b \in \mathcal{B}, \forall t \in \mathcal{T}. \tag{22}$$

where $\mathcal{B}$, $\mathcal{L}$, $\mathcal{G}$, and $\mathcal{T}$ denote the set of transmission buses b, transmission lines l, generators g, and time slots t. The objective function (14) is to minimize the load curtailment cost over all the sets of buses and the scheduling horizon where $\text{LC}_{b,t}^s$ denotes the load curtailment in bus b in time t in scenario s and $\text{VOLL}_{b,t}$ denotes the value of loss load. The optimization is subject to the following constraints. The DC power flow constraints of the transmission lines l connecting bus b and b' is captured in (15) where the scenario based outage status of the line l is represented by a binary parameter $\delta_{l,t}^s$. In particular, if the line is potentially damaged by the modeled wildfire, i.e., $\delta_{l,t}^s = 1$, there is no power flow on the line. Power balance constraint in bus b is captured in (16) where the power $P_{g,b,t}^s$ generated by g in b, minus the bus power demand $P_{d,b,t}$, plus load curtailment $\text{LC}_{b,t}^s$, equals the total power flowing out of b. Additionally, the load curtailment at any bus must remain within the limitations of the total demand at that bus, which is presented in (17). The power generated by g is constrained by its minimum and maximum capacity as in (18). The power flow over the line l is constrained by its thermal capacity $\overline{P}_l$ as in (19). On a similar note, the upper and lower limit constraints of the bus phase angle $\theta_{b,t}^s$ are described in (20). Furthermore, the limitations $RU_{g,b}, RD_{g,b}$ of the generators' ramping up and down rates are furnished in (21) and (22) respectively. Note that our framework can also apply to power distribution network where DC power flow constraints are replaced by the DisTFlow model considering line outage status [40].

4.2.3 The Expected Power System Damage Cost: The expected damage cost of power systems [41] for a given set of wildfire motivated outage scenarios S is calculated as:

$$ECOST = \sum_{s \in \mathcal{S}} \pi_s \times \text{cost}_s, \tag{23}$$

where cost_s is obtained by solving the optimal response of the power grid against the wildfire motivated outage scenario s, e.g. solving optimization problems (14)-(22) for the case of transmission networks. Hence, the $ECOST$ metric, in addition to estimated infrastructure damage costs, can aid utility decisions of wildfire mitigation vs. restoration, i.e., informing the important question: should the utility use the "let-burn" strategies, since oftentimes the utility is burdened with the economic decision of either fighting wildfires or employing the "let-burn strategy" where the wildfire is allowed to burn and damages are rebuilt/restored [42]. If the firefighting costs are greater than the expected damage costs (operational, infrastructural and otherwise), the utility could utilize the "let-burn" strategy.

5 Numerical Results

5.1 Simulation Setup

We consider an area covering approximately $200km^2$ in northern California and spanning latitudes $38^\circ 49' 17.616'' N$ to $40^\circ 46' 7.14'' N$, and longitudes $120^\circ 11' 52.8'' W$ to $122^\circ 43' 55.2'' W$. The chosen area reflects homogeneous climate yet spatially diverse in fuel and vegetation as illustrated in Fig. 15 detailed in Appendix 8.3. The STWIP was trained and validated using a 70% and 30% split training data of 10,900 samples, and compared to other data-based conventional baselines [43, 44] including decision tree, boosted decision tree, and linear regression. We first provide the wildfire estimation results over the studied area to illustrate the effectiveness of the first stage of the framework, i.e., the STWIP model.

5.2 Wildfire Estimation Analysis

The performance analysis in Fig. 6 shows the average accuracy for training and validation of the STWIP was (98.31% and 97.0%), while the boosted decision tree was (93.27% and 92.0%), both outperforming other baselines. Also, the proposed STWIP achieves the

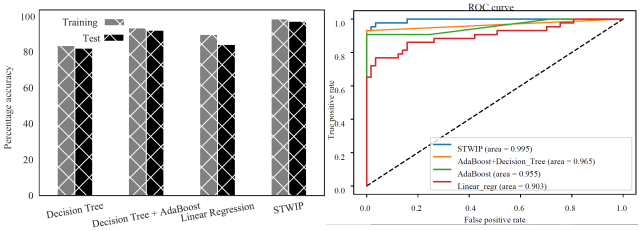

Fig. 6: Accuracy of baselines

Accepted for publication in IET Generation, Transmission & Distribution, January 2022

best performance with an Area Under the Receiver Operating Characteristic curve (AUC) of 0.995. Note that the AUC describes the model trade-off in terms of sensitivity and specificity. This performance is followed again by the boosted + tree algorithm with an AUC of 0.965 and the regression with an AUC of 0.903 respectively.

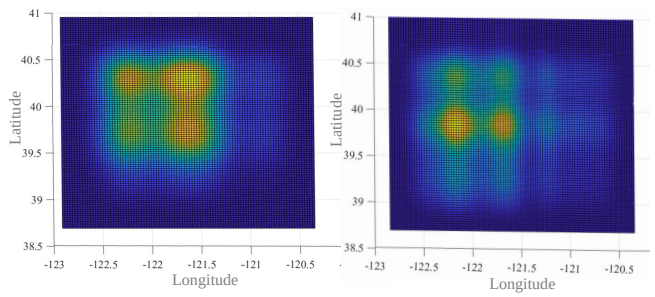

Fig. 7: Test Year: Actual (left) vs. predicted spatial ignition pattern

Next, we test STWIP with the 2018 year, comparing results with the actual wildfire occurrence currently available in [45]. In the test data we use the 15^{th} day of the month as it is representative of its wildfire characteristics. Thus, we seek to obtain similar patterns of spatial density and temporal distribution. Results in Fig. 7 show that

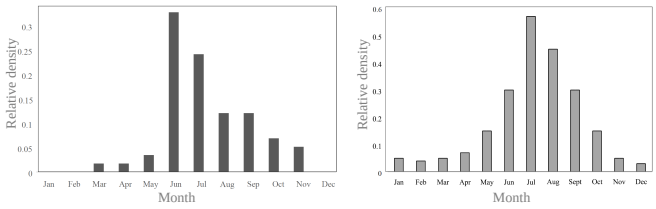

Fig. 8: Test Year: Actual(left) vs. predicted temporal ignition pattern

predicted hotspots are similar to the actual historical test year, clustered between latitudes and longitudes (39° 30' 00" N , 122° 30' 00.0000" W) and (39° 30' 00.0000" N , 121° 30' 00.0000" W). The central valley area of northern California has less ignition clusters, which is attributed to limited elevation and fuel. Similarly, the temporal results are analyzed monthly as furnished in Fig.8, showing that the estimated temporal distribution well follows the test year's actual temporal wildfire distribution (approximately Gaussian). Hence, by employing the STWIP for analysis as opposed to the conventional utility predefined fire threat areas and fire threat levels as detailed in Appendix 8.7, power systems can further improve wildfire forecast and analysis towards actual expectations.

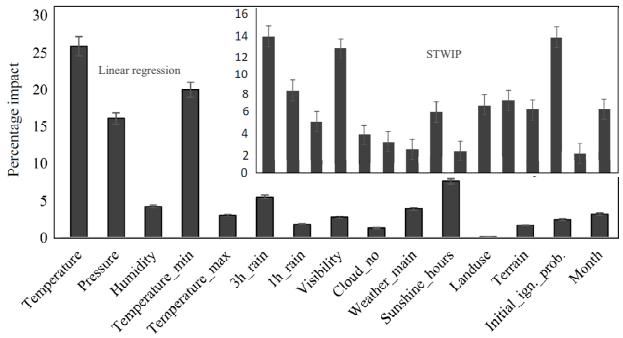

Fig. 9: Influence of wildfire predictor variables: STWIP captures the magnitude of this influence better than the widely utilized linear regression. For instance, the influence of landuse and terrain which are well known influential factors in wildfire occurrence

The percentage weighted impact of WPVs on the wildfire ignition status is presented in Fig 9. In particular, the WPVs are evaluated based on their weighted influence on wildfire occurrence. Terrain and temperature, and cloud type and historical ignition, have the highest and least influence, respectively. Also, humidity seemingly influenced daily wildfire ignition maps produced by the predictor especially in the central valley of northern California. This suggests which measurement types (sensors in monitoring corridors) that the power utility should invest for enhancing situational awareness against wildfire. The performance of STWIP is further underlined as linear methods such as regression do not well capture terrain which is indeed a high impact feature [46].

5.3 Illustrating Wildfire Aware Power Grid Operation Analysis

Conventionally, utility often uses region-scale and deterministic threat level analysis as discussed in Section 1.1 and detailed in Appendix 8.7. In this situation as further illustrated by Fig. 10,

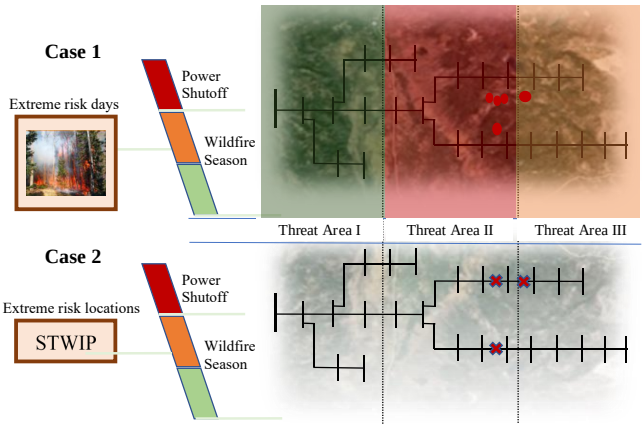

Fig. 10: Illustration of the cases

as seen in the "conservative" utility case, the utility will have an extreme alert in the red area since there are more wildfire threats as opposed to the elevated threat area (orange highlight). The customers in the area with extreme alert will have their power shut off for the duration of the wildfire threat, including customers up north (relatively farther) from the wildfire threat cluster. The magnitude of the shut off can be visualized given the size of the predefined threat areas in a sample utility wildfire awareness issue as shown in Fig. 18 in Appendix 8.7. However, the potential ignition map and spread parameters provided by the first stage estimation model can be used to analyze the risk of over de-energization motivated by power component failure-ignited wildfires and the risk of outages induced by exogenous wildfire. With the granularity in spatial detail of the wildfire potential probability maps, the spread model, and the proposed risk assessment, the utility can optimize the time before shut off is necessary in exogenous fires, and also emulate the distance between a potential ignition location (ignitable location) and the power equipment in endogenous/equipment-induced wildfires. The analysis is conducted on a 24-bus test system mapped to span the length and breath of the studied area as detailed in Appendix 8.6, however, this analysis can be done on any transmission or distribution system given complete system details. We consider two case studies which deviate from the power system normal operation when there are no wildfire threats. In case 1, the test system is simulated with the current conventional "conservative" utility approach of threat area and levels discussed in the Section 1.1 and detailed in

Table 2 Wildfire Motivated De-energization

Case Study	Transmission Line Outages	Generator Outages
Case 1	L1-4, L6-8, L14, L19, L24-33	G1-4, G15-29
Case 2	L4, L8, L19, L23-24, L28, L31-33	None

Accepted for publication in IET Generation, Transmission & Distribution, January 2022

Appendix 8.7. In this case, all the power components located in the pre-defined elevated threat area as illustrated in Appendix 8.7 are intentionally outaged whether or not they are in the direct vicinity of high wildfire potential. This simulates current utility procedure to prevent endogenous wildfires [10]. In case 2, the wildfire analysis and test system de-energization is based on the wildfire potential ignition map produced by STWIP as described in Section 4 aiming to improve spatial granularity and optimize (shorten) the time span of utility de-energization. The data used in simulation is based on Nov. 10, 2018. The value of lost load is set to 1000 $/MWh. Details of the components that are out of service in the three case studies are shown in Table 2.

5.3.1 Assessing risk of outages induced by exogenous wildfire: For exogenous wildfire induced outage risk analysis, the probabilistic ignition map is used to generate wildfire ignition scenarios and simulated spreading pattern, thus modeling exogenous wildfire-induced damages on power grid components. The expected damage cost, ECOST, as illustrated in Fig. 11, represents the aggregate analysis for one operational year of the test system in the studied area. It shows that the power system is highly vulnerable during summer time from June to September, and quite low during winter time from December to March. However, the risk of wildfire induced outage still exists during non-summer times, which can be explained by the impacts of the time independent WPVs such as landuse and terrain. Hence, an efficient allocation of utility wildfire monitoring resources should be based on spatio-temporal analysis of wildfire occurrence, e.g., monitoring grid and vegetation should be done more frequently during high risk period.

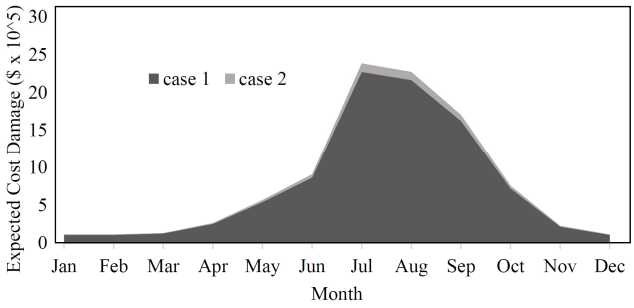

Fig. 11: Expected damage cost over the period of one year: showing sustained wildfire risk during non-summer months

5.3.2 Enhancing de-energization decision for mitigating power component failure-ignited wildfires: Wildfires can be ignited by electric power line faults that cause arcing in a high-heat release of energy. Such incidents are majorly caused by ignitable vegetation contacting power lines. Indeed, the correlation between the wildfire ignition probability map and electric power failures motivates the use of proactive de-energization of equipment as a preventive measure [28]. We aim to illustrate the improvements in de-energization using the proposed STWIP, which is more granular and stochastic, over conventional utility approach. The proposed framework aids in enhancing de-energization and estimating the potential cost of wildfire occurrence as detailed further.

The total system energy consumption, total loadshed, and loadshed-bus localization of the three cases are shown in Fig. 12. The total energy demand of the system is 54358.679 MWh, with case 1 supplying 29449.051 MWh due to large amounts of load shedding, 45.8%, resulting from the conventional threat area and threat level methods. Relative to case 2, the power grid response avoids a large amount, 19798 MWh, of unnecessary load shedding. Hence, a more detailed wildfire potential ignition map provided by the proposed granular analysis results in less conservative shutoff, i.e., only components in the high wildfire vicinity are proactively de-energized to prevent component failure-caused wildfire [28]. Table 3 presents

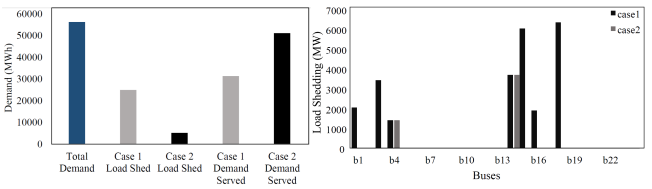

Fig. 12: Demand served and load shedding for cases 1 and 2: illustrating that a detailed wildfire potential ignition map provided by the proposed power grid wildfire risk assessment model results in less conservative proactive de-energization

Table 3 Costs for Cases 1 AND 2 ($)

	Load Shedding Cost ($)	Generation Cost ($)
Case 1	181,591.25	537,969.01
Case 2	37,263.75	537,991.32

load shedding cost, and generation cost for all cases. For the normal system operation, there are no load shed costs and generation costs are $568,084.40 The total costs for case 1 is high due to the amount of load shed and the increase in production of expensive online generators.

In addition, the framework aids improve the resilience of the system by spatio-temporally informing the disaster progression phase of the resilience trapezoid as illustrated in Fig 13, hence reducing the "dip" in the resilience curve [47]. Specifically, in case 1, a large

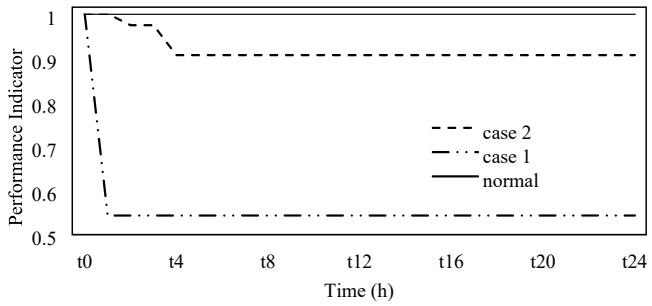

Fig. 13: Profile of load served in the system. The proposed power grid wildfire risk assessment model aids in enhancing system robustness and hence resilience, as evident in case 2 as opposed to case 1

and sudden drop of the percentage load served (performance indicator) is observed. This is because without spatio-temporal analysis, the utility performs conservative forced outages as soon as a wildfire threat is observed in their pre-defined regional threat areas, which in this simulation is set to the beginning of the scheduling horizon at $t^* = 0$. The percentage load served in case 2 is observed to reduce over time. This is possible due to the improved granularity provided by spatio-temporal analysis where expectations of wildfire parameters such as distance, spread rate, and the critical response time have been pre-estimated as discussed in Section 4.2.1. Hence, with a grasp of the expected critical response times, the utility operations have increased and informed time flexibility in forcing component outages.

6 Conclusion

This paper proposed a comprehensive spatio-temporal framework for power system wildfire risk analysis. The framework includes two sequential models, where the first model estimates the granular and spatio-temporal potential wildfire probability and spread

Accepted for publication in IET Generation, Transmission & Distribution, January 2022

based on influential parameters such as vegetation and fuel, wind speed, geographical and meteorological variables, while the second model leverages the estimated probabilistic ignition maps in order to analyze system risk from exogenous wildfire and to enhance power system de-energization in mitigating endogenous fires induced by power equipment failures. Numerical results show that lower forced electricity outages to customers can be achieved by increased granularity in spatial locations in utility service areas. Hence, the framework significantly improves utility de-energization decision compared to the current "conservative" threat area approach In addition, the framework aids to improve system resilience and utility revenue and prioritize resource allocation given increased localization of high wildfire potential. Future work will entail using the proposed model as a base in proposing a self-sufficient model for complete wildfire prediction and detection for electric power utilities using recent state-of-the-art sensor developments and designs in wildfire detection. Part of these future studies are already formulated but not included in this paper to enable a concise and clear exposition.

7 References

1 E. O. of the President. Council of Economic Advisers, *Economic Benefits of Increasing Electric Grid Resilience to Weather Outages*. The Council, 2013.
2 [Online]. Available: https://www.iii.org/table-archive/21424
3 B. C. D. Attorney, "The camp fire public report: A summary of the camp fire investigation," 2020.
4 [Online]. Available: https://www.utilitydive.com/news/the-hard-choice-californias-wildfires-have-forced-on-its-utilities-and-a/548614/
5 [Online]. Available: https://www.fire.ca.gov/media/hsviuuv3/cal-fire-2020-fire-siege.pdf
6 [Online]. Available: https://www.latimes.com/california/story/2021-11-01/amid-federal-probe-in-dixie-fire-pacific-gas-electric-faces-1-billion-in-losses
7 [Online]. Available: https://inciweb.nwcg.gov/incident/7690/
8 J. D. Horel and X. Dong, "An evaluation of the distribution of remote automated weather stations (raws)," *Journal of Applied Meteorology and Climatology*, vol. 49, no. 7, pp. 1563–1578, 2010.
9 D. P. Tyndall and J. D. Horel, "Impacts of mesonet observations on meteorological surface analyses," *Weather and Forecasting*, vol. 28, no. 1, pp. 254–269, 2013.
10 [Online]. Available: https://www.cnbc.com/2019/10/08/pge-to-cut-off-power-to-nearly-800000-customers-to-reduce-wildfire-risk.html
11 [Online]. Available: https://leginfo.legislature.ca.gov/faces/billTextClient.xhtml?bill_id=201920200AB1054
12 [Online]. Available: https://fpi.sdgeweather.com
13 K. Xu, X. Zhang, Z. Chen, W. Wu, and T. Li, "Risk assessment for wildfire occurrence in high-voltage power line corridors by using remote-sensing techniques: A case study in hubei province, china," *International journal of remote sensing*, vol. 37, no. 20, pp. 4818–4837, 2016.
14 D. Chaparro, M. Vall-Llossera, M. Piles, A. Camps, C. Rüdiger, and R. Riera-Tatché, "Predicting the extent of wildfires using remotely sensed soil moisture and temperature trends," *IEEE journal of selected topics in applied earth observations and remote sensing*, vol. 9, no. 6, pp. 2818–2829, 2016.
15 D. N. Trakas and N. D. Hatziargyriou, "Optimal distribution system operation for enhancing resilience against wildfires," *IEEE Transactions on Power Systems*, vol. 33, no. 2, pp. 2260–2271, 2018.
16 A. A. Alencar, L. A. Solórzano, and D. C. Nepstad, "Modeling forest understory fires in an eastern amazonian landscape," *Ecological Applications*, vol. 14, no. sp4, pp. 139–149, 2004.
17 J. P. Prestemon, M. L. Chas-Amil, J. M. Touza, and S. L. Goodrick, "Forecasting intentional wildfires using temporal and spatiotemporal autocorrelations," *International Journal of Wildland Fire*, vol. 21, no. 6, pp. 743–754, 2012.
18 R. A. Bradstock, J. Cohn, A. M. Gill, M. Bedward, and C. Lucas, "Prediction of the probability of large fires in the sydney region of south-eastern australia using fire weather," *International Journal of Wildland Fire*, vol. 18, no. 8, pp. 932–943, 2010.
19 H. Zhang, X. Han, and S. Dai, "Fire occurrence probability mapping of northeast china with binary logistic regression model," *IEEE Journal of Selected Topics in Applied Earth Observations and Remote Sensing*, vol. 6, no. 1, pp. 121–127, 2013.
20 J. Arganaraz, A. Lighezzolo, K. Clemoveki, D. Bridera, J. Scavuzzo, and L. Bellis, "Operational meteo fire risk system based on space information for chaco serrano," *IEEE Latin America Transactions*, vol. 16, no. 3, pp. 975–980, 2018.
21 S. Lall and B. Mathibela, "The application of artificial neural networks for wildfire risk prediction," in *2016 International Conference on Robotics and Automation for Humanitarian Applications (RAHA)*. IEEE, 2016, pp. 1–6.
22 L. Vilar, D. G. Woolford, D. L. Martell, and M. P. Martín, "A model for predicting human-caused wildfire occurrence in the region of madrid, spain," *International Journal of Wildland Fire*, vol. 19, no. 3, pp. 325–337, 2010.
23 A. Malik, M. R. Rao, N. Puppala, P. Koouri, V. A. K. Thota, Q. Liu, S. Chiao, and J. Gao, "Data-driven wildfire risk prediction in northern california," *Atmosphere*, vol. 12, no. 1, p. 109, 2021.
24 J. Storer and R. Green, "Pso trained neural networks for predicting forest fire size: a comparison of implementation and performance," in *2016 international joint conference on neural networks (IJCNN)*. IEEE, 2016, pp. 676–683.
25 A. Jaafari, E. K. Zenner, M. Panahi, and H. Shahabi, "Hybrid artificial intelligence models based on a neuro-fuzzy system and metaheuristic optimization algorithms for spatial prediction of wildfire probability," *Agricultural and forest meteorology*, vol. 266, pp. 198–207, 2019.
26 H. Liang, M. Zhang, and H. Wang, "A neural network model for wildfire scale prediction using meteorological factors," *IEEE Access*, vol. 7, pp. 176 746–176 755, 2019.
27 Y. Li, H. Mulyono, Y. Chen, Z. Lu, and D. Chan, "Rtfps: An interactive map that visualizes and predicts wildfires in the us," *arXiv preprint arXiv:2105.10880*, 2021.
28 N. Rhodes, L. Ntaimo, and L. Roald, "Balancing wildfire risk and power outages through optimized power shut-offs," *arXiv preprint arXiv:2004.07156*, 2020.
29 B. Ansari and S. Mohagheghi, "Optimal energy dispatch of the power distribution network during the course of a progressing wildfire," *International Transactions on Electrical Energy Systems*, vol. 25, no. 12, pp. 3422–3438, 2015.
30 M. Choobineh, B. Ansari, and S. Mohagheghi, "Vulnerability assessment of the power grid against progressing wildfires," *Fire Safety Journal*, vol. 73, pp. 20–28, 2015.
31 M. E. Chambers, P. J. Fornwalt, S. L. Malone, and M. A. Battaglia, "Patterns of conifer regeneration following high severity wildfire in ponderosa pine–dominated forests of the colorado front range," *Forest Ecology and Management*, vol. 378, pp. 57–67, 2016.
32 B. K. Blaylock, J. D. Horel, and C. Galli, "High-resolution rapid refresh model data analytics derived on the open science grid to assist wildland fire weather assessment," *Journal of Atmospheric and Oceanic Technology*, vol. 35, no. 11, pp. 2213–2227, 2018.
33 N. Hamadeh, B. Daya, A. Hilal, and P. Chauvet, "An analytical review on the most widely used meteorological models in forest fire prediction," in *2015 Third International Conference on Technological Advances in Electrical, Electronics and Computer Engineering (TAEECE)*. IEEE, 2015, pp. 239–244.
34 M.-A. Parisien, S. Snetsinger, J. A. Greenberg, C. R. Nelson, T. Schoennagel, S. Z. Dobrowski, and M. A. Moritz, "Spatial variability in wildfire probability across the western united states," *International Journal of Wildland Fire*, vol. 21, no. 4, pp. 313–327, 2012.
35 M. A. Finney, C. W. McHugh, I. C. Grenfell, K. L. Riley, and K. C. Short, "A simulation of probabilistic wildfire risk components for the continental united states," *Stochastic Environmental Research and Risk Assessment*, vol. 25, no. 7, pp. 973–1000, 2011.
36 J. Bishop, "Technical background of the fireline assessment method (flame)," in *In: Butler, Bret W.; Cook, Wayne, comps. The fire environment–innovations, management, and policy; conference proceedings. 26-30 March 2007; Destin, FL. Proceedings RMRS-P-46CD. Fort Collins, CO: US Department of Agriculture, Forest Service, Rocky Mountain Research Station. CD-ROM. p. 27-74*, vol. 46, 2007.
37 E. I. Koufakis, P. T. Tsarabaris, J. S. Katsanis, C. G. Karagiannopoulos, and P. D. Bourkas, "A wildfire model for the estimation of the temperature rise of an overhead line conductor," *IEEE transactions on power delivery*, vol. 25, no. 2, pp. 1077–1082, 2010.
38 M. Choobineh and S. Mohagheghi, "Power grid vulnerability assessment against wildfires using probabilistic progression estimation model," in *2016 IEEE Power and Energy Society General Meeting (PESGM)*. IEEE, 2016, pp. 1–5.
39 J.-L. Rossi, A. Simeoni, B. Moretti, and V. Leroy-Cancellieri, "An analytical model based on radiative heating for the determination of safety distances for wildland fires," *Fire Safety Journal*, vol. 46, no. 8, pp. 520–527, 2011.
40 M. E. Baran and F. F. Wu, "Network reconfiguration in distribution systems for loss reduction and load balancing," *IEEE Trans. on Power delivery*, vol. 4, no. 2, pp. 1401–1407, 1989.
41 E. Vugrin, A. Castillo, and C. Silva-Monroy, "Resilience metrics for the electric power system: A performance-based approach," *Report: SAND2017-1493*, 2017.
42 R. M. Houtman, C. A. Montgomery, A. R. Gagnon, D. E. Calkin, T. G. Dietterich, S. McGregor, and M. Crowley, "Allowing a wildfire to burn: estimating the effect on future fire suppression costs," *International Journal of Wildland Fire*, vol. 22, no. 7, pp. 871–882, 2013.
43 A. Jaafari, E. K. Zenner, and B. T. Pham, "Wildfire spatial pattern analysis in the zagros mountains, iran: A comparative study of decision tree based classifiers," *Ecological informatics*, vol. 43, pp. 200–211, 2018.
44 M. Rodrigues, A. Jiménez-Ruano, D. Peña-Angulo, and J. De la Riva, "A comprehensive spatial-temporal analysis of driving factors of human-caused wildfires in spain using geographically weighted logistic regression," *Journal of environmental management*, vol. 225, pp. 177–192, 2018.
45 [Online]. Available: https://www.fire.ca.gov/incidents/2018/
46 M. Calviño-Cancela, M. L. Chas-Amil, E. D. García-Martínez, and J. Touza, "Interacting effects of topography, vegetation, human activities and wildland-urban interfaces on wildfire ignition risk," *Forest Ecology and Management*, vol. 397, pp. 10–17, 2017.
47 A. Umunnakwe, H. Huang, K. Oikonomou, and K. Davis, "Quantitative analysis of power systems resilience: Standardization, categorizations, and challenges," *Renewable and Sustainable Energy Reviews*, vol. 149, p. 111252, 2021.
48 [Online]. Available: https://www.academia.edu/13981064/Data_for_the_IEEE_24_bus_Reliability_Test_System
49 K. Carbon and B. DAgostino, "Catastrophic risk mitigation through analytics: Wildfire threat index," Sempra Energy and San Diego Gas & Electric, Tech. Rep., 2015.
50 SDG&E, "San diego gas & electric company fire prevention plan."

8 APPENDIX

8.1 Spatial Features Details

We assume that land-use data contains information on fuel type, fuel load, fuel continuity as illustrated in Table 1 while terrain informs the topography of the ecoregion. The land-use and terrain are examples of spatial features and usually do not change significantly over the short-term, hence the name static. Land-use refers to the natural vegetation and the various ways in which humans make use of and manage the land and its resources. The terrain represents the topography of the geographical area. Hence, input features employed are not exhaustive but motivated from wildfire studies.

8.2 Same Climate Assumption

In this work, we assume same climate distribution over the period which we collect historical data for analysis. This assumption is enabled by similar distribution in spatial and temporal data. In the said period, the later is approximately Gaussian, while the former is as furnished in Fig. 14.

Fig. 14: Same Climate Assumption: Similar distribution of Historical data-points Latitude and Longitude.

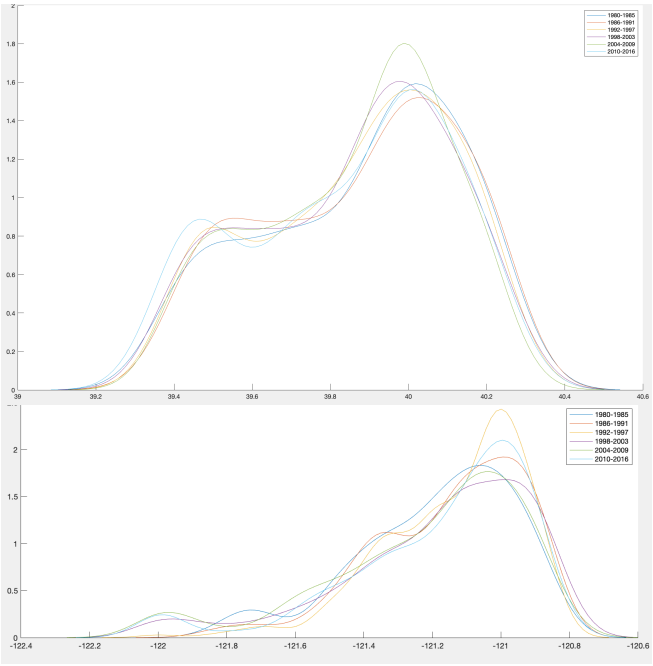

8.3 Spatio-Temporal Wildfire Estimation Model: Setup

Landuse was obtained from the NOAA's HRRR model and ranges from evergreen needleleaf forest to barren tundra, assigned values [1, 20], while Terrain input gives insight into the topography and elevation of the area with values in the range [6, 2603] meters as shown in Fig. 15. Temporal variables were obtained from the Open Weather Map database by building an application programming interface scrapper in python, to make data requests to the open weather map online weather database using the $http$ protocol. Requested meteorological data includes temperature levels, rain, humidity, cloud, atmospheric pressure, visibility, month and sunshine hours, where numerical values are assigned to qualitative features, for instance, the daily weather types (clear, cloudy, hazy, drizzly, rainy) are assigned real values in the ratio [0.1, 0.3, 0.5, 0.7, 0.8] respectively. Historical wildfire ignition records were obtained for the multi-year period of analysis (1996-2016,2018) from the U.S. Geographical Survey database and provides the samples of the training and test data, respectively.

8.4 Temporal Probability Details

The temporal probabilities of wildfire ignition is also calculated from historical data with the assumption of a same climate period as shown in Fig.16.

8.5 The STWIP Algorithm

Algorithm 1 Batch Learning Based STWIP

Given a training set $(\mathbf{x}_1, y_1), ..., (\mathbf{x}_n, y_n)$ with features in instances $\mathbf{x}_i \in R^n$, with label $y_i \in \{0, 1\}$
Input(X,Y): A set of labeled input features [temp, ..., month], of training samples θ, batch size b
Output: The spatio-temporal ignition probability maps.
Hyper-parameter selection
function $Predictor\_Training$(X, Y)
    Shuffle ←enabled
    count_max ← $\frac{\theta}{b}$
    count ← 0
    while count < count_max **do**
        for batch b in θ **do**
            STWIP ← DNN learns (b×[temp, ..., month])
            count ++
        end for
    end while
    Compute accuracies
    Compute the ROC AUC metrics
    Apply STWIP to test samples
return Wildfire potential ignition maps of $\pi_{i,j}$
end function

The trained STWIP, as presented in Algorithm 1, is then validated and utilized in the prediction for unlabelled test samples for a future period j. When the algorithm ends, the probability map of potential ignitions, $\pi_{i,j}$, is returned.

8.6 Mapping Bulk Power Grid to the Wildfire Potential Map

The IEEE 24-bus reliability test system [48] that includes 24 buses, 38 lines and 33 generating units is aligned to the ignition probability map as shown in Fig. 17. Also, to illustrate conventional power utility wildfire practices, the grid is divided into fire threat areas with extreme, elevated, and normal threat levels, while spatio-temporal analysis employs the most probable generated scenarios.

8.7 Utility-Employed Predefined Fire Threat Areas and Levels

Electric power utilities have carried out ground breaking work in modeling wildfire occurrence, including developing analytical tools such as the Fire Potential Index (FPI) and more [49]. These indices, for instance the FPI, calculated at district level corresponding to three levels of wildfire threat alert, are efficient for planning decisions, however, they start to fall short in the day to day operational decisions for utilities as spatio-temporal granularity is lost in these methods i.e., the use of pre-defined wide threat areas and few (extreme, elevated, normal) threat levels.

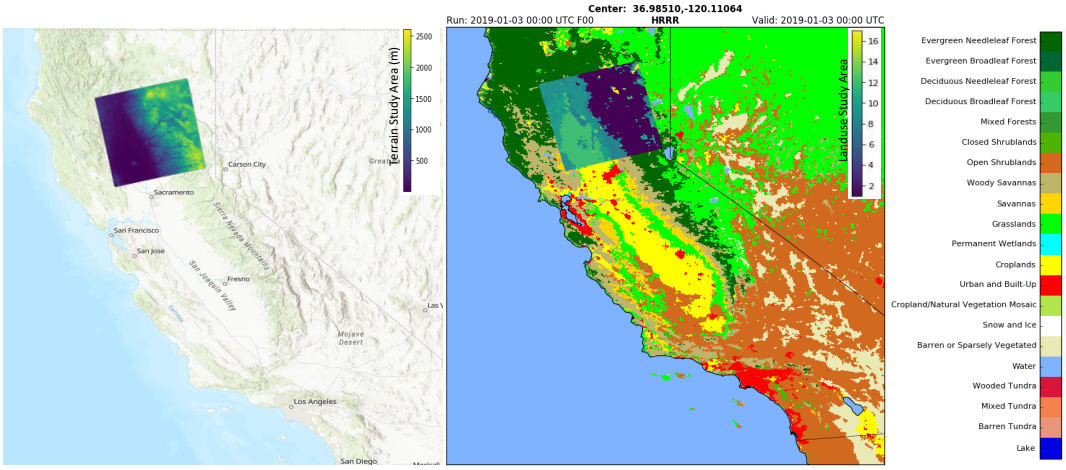

Fig. 15: The spatial features of studied geographical area: terrain (left) and land-use (right)

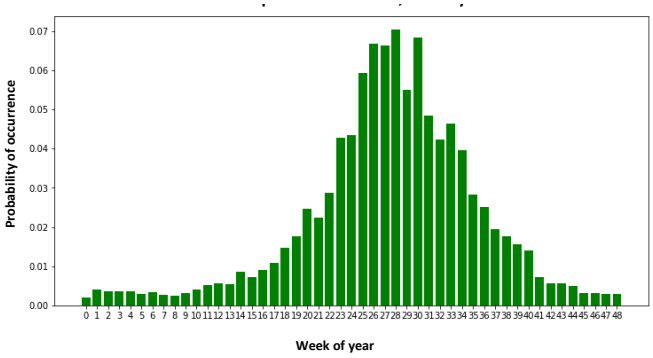

Fig. 16: Weekly Temporal Distribution of Historical Wildfire Occurrence

In particular, the challenges posed by current utility techniques include the use of Fire Threat Areas (FTAs), Fire Threat Levels (FTLs), the independent analysis of the Wildfire Predictor Variables (WPVs), and the exclusion of adequate past wildfire characteristics in analysis. As stated by Brian D'Agostino, SDGE's director of fire science and climate adaptation: "We need to understand what the weather is doing in every canyon, every ridgetop all across the back-country to really bring that level of customer safety and customer service". Thus, the use of FTAs and FTLs can introduce ambiguity in utility analysis, such as the over allocation of resources, excess load shedding in risk assessment, and lengthened forced outages to customers, since the pre-defined area may not be granular enough for operational wildfire analysis. Furthermore, the independent analysis of wildfire predictor variables introduces errors in estimation due to the exclusion of the effects of the interactions between these variables. For instance, for utility operations, when certain conditions (e.g., relative humidity $\leq$ 15%, sustained winds and gusts $\geq$ 25mph and 35 mph respectively, for a duration $\geq$ 6 hours) are met, operational decisions e.g., all reclosers being turned off, sensitive relay settings being enabled [50], are taken. However, these assessments of environmental conditions are made independently, leaving little room for evaluating how the interactions between variables drive wildfire potential. Moreover, data obtained from historic events provide increased information on spatial wildfire characteristics as demonstrated in this work.

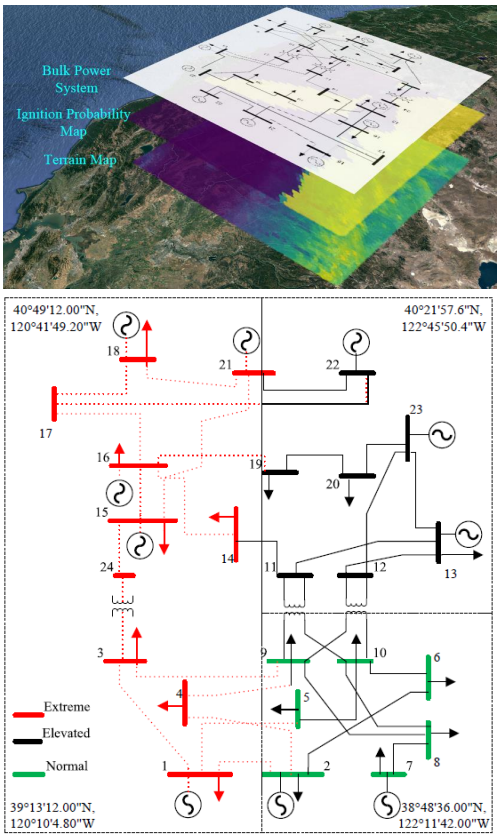

Fig. 17: IEEE 24-bus mapping into three wildfire threat areas

IET Generation, Transmission & Distribution, pp. 1–13

Accepted for publication in IET Generation, Transmission & Distribution, January 2022

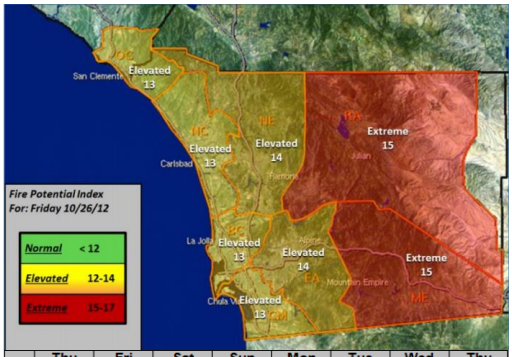

	Thu 10/25	Fri 10/26	Sat 10/27	Sun 10/28	Mon 10/29	Tue 10/30	Wed 10/31	Thu 11/01
ME	Normal 11	Extreme 15	Elevated 13	Elevated 12	Normal 11	Normal 11	Normal 11	Normal 10
RA	Normal 11	Extreme 15	Elevated 13	Elevated 12	Normal 11	Normal 11	Normal 11	Normal 10
EA	Normal 10	Elevated 14	Elevated 12	Normal 11	Normal 11	Normal 10	Normal 10	Normal 10
NE	Normal 10	Elevated 14	Elevated 12	Normal 11	Normal 11	Normal 10	Normal 10	Normal 10
OC	Normal 10	Elevated 13	Normal 11	Normal 11	Normal 10	Normal 9	Normal 9	Normal 9
NC	Normal 10	Elevated 13	Normal 11	Normal 11	Normal 10	Normal 9	Normal 9	Normal 9
BC	Normal 10	Elevated 13	Normal 11	Normal 11	Normal 10	Normal 9	Normal 9	Normal 9
CM	Normal 10	Elevated 13	Normal 11	Normal 11	Normal 10	Normal 9	Normal 9	Normal 9

Fig. 18: A sample SDG&E wildfire awareness issue

Accepted for publication in IET Generation, Transmission & Distribution, January 2022